Fermi National Accelerator Laboratory

FERMILAB-TM-2013

Test of DEP Hybrid Photodiodes

A. Baumbaugh, M. Binkley, J. Elias, J. Freeman, D. Green, S. Hansen, C. Rivetta, A. Ronzhin and R. Tschirhart

Fermi National Accelerator Laboratory
P.O. Box 500, Batavia, Illinois 60510

P. Cushman and A. Heering

University of Minnesota
Minneapolis, Minnesota

August 1997

Disclaimer

This report was prepared as an account of work sponsored by an agency of the United States Government. Neither the United States Government nor any agency thereof, nor any of their employees, makes any warranty, express or implied, or assumes any legal liability or responsibility for the accuracy, completeness or usefulness of any information, apparatus, product or process disclosed, or represents that its use would not infringe privately owned rights. Reference herein to any specific commercial product, process or service by trade name, trademark, manufacturer or otherwise, does not necessarily constitute or imply its endorsement, recommendation or favoring by the United States Government or any agency thereof. The views and opinions of authors expressed herein do not necessarily state or reflect those of the United States Government or any agency thereof.

Distribution

Approved for public release: further dissemination unlimited.

Fermi National Accelerator Laboratory

FERMILAB-TM-2013

Test of DEP Hybrid Photodiodes

A. Baumbaugh, M. Binkley, J.Elias, J.Freeman, D.Green,
S.Hansen, C.Rivetta, A.Ronzhin, R.Tschirhart

Fermi National Accelerator Laboratory
P.O.Box 500, Batavia, Illinois 60510

P.Cushman, A.Heering

University of Minnesota
Minneapolis, Minnesota

August 1997

Operated by Universities Research Association Inc. under Contract No. DE-AC02-76CHO3000 with the United States Department of Energy

Fermi National Accelerator Laboratory

FERMILAB-TM-2013

A.Baumbaugh, M.Binkley, J.Elias, J.Freeman, D.Green,
S.Hansen, C.Rivetta, A.Ronzhin, R.Tschirhart,
Fermilab

P.Cushman, A.Heering
University of Minnesota, Minneapolis, Minnesota

TEST OF DEP HYBRID PHOTODIODES

INTRODUCTION

The goal of the measurement was to study some parameters of DEP HYBRID PHOTODIODES (HPD) [1], and to check its performance for CMS calorimetry at LHC [2]. The principle of the HPD operation is described, for example, in ref. [3] The schematic view of the HPD is shown in fig. 1. The HPD is vacuum photo device composed of photocathode (PC) and a silicon PIN diode (Si) as multiplication system in a very close proximity geometry. The distance between PC and Si is of the order of several mm and has an electric field < 10 kV. The photoelectrons emited by the photocathode multiply by a factor of several thousand in the silicon and the charge is collected on the HPD's anode. Several types of HPD's were tested. There was a single channel HPD, called "E-type" with p-side of the silicon facing the HPD's photocathode and two multipixel HPD (DEP) namely a 25 pixel HPD and a 7 pixel HPD. Both were of "T-type" structure with n-side of silicon facing the photocathode.

SETUP

The main part of the setup was a nitrogen laser with a shifted wavelength of 440 nm, 10 Hz frequency and a pulse duration of 15 ns. The laser light was transported to the HPD by a 1 mm clear fiber. The amount of laser light was changed by rotating wheels with fixed light attenuation. The dynamic range of the HPD + AMP + ADC was about 1000. To make the non uniformity measurement across the photocathode, the HPD was mounted on a movable stage under control of a computer. The accuracy of the adjustment of the fiber across the sensitive area of the HPD was better than 100 um. The setup is shown in fig.2. We also used a blue (430 nm) light emitting diode (LED) with a 1 mm clear optical fiber transmitting the light to the HPD in part of measurements. The LED light pulse duration was less than 10 ns.

MEASUREMENTS

For each type of HPD the following parameters were measured:

1. Gain.
2. Linearity.
3. Nonuniformity.
4. Timing properties.
5. Counting rate capabilities.

Some other measurements were performed to check possible aging of HPD's, the influence of a magnetic field on the HPD and crosstalk for multipixel devices. We made some estimation of the lowest level of light signal which is possible to separate from the HPD noise. The point was to see if the signal for a minimum ionizing particle traversing the CMS calorimeter which is of approximately 10 phe, or around 1 GeV of the energy loss in the calorimeter, can be observed.

The data will be presented in the indicated sequence for each type of HPD.

SINGLE CHANNEL HPD

A schematic view of a single channel HPD is shown in fig.3. The HPD has a 25 mm diameter phothocatode (PC) and the same size silicon diode with the p-side facing the PC. The recommended supply voltage scheme was applied with the output signal of negative polarity with AC coupling. The signal amplitude as a function of the high voltage applied to PC and the bias applied to the silicon are presented in fig.4. The data are consistent with the DEP specifications. They show the threshold caused by the silicon dead layer and the linear dependence on high voltage (HV). The gain value is around 2000 for HV=8 kV. A small variation of the gain dependence on the bias voltage (for bias more than 30 V) is also presented, indicating full depletion.

The measurements of the linearity were done using the setup designed by N.Hogan and J.Krider of Fermilab. The observed nonlinearity was less than +/- 0.5% for the dynamic range 1-10000 and was largely caused by the amplifier's nonlinearity.

The timing measurements for the HPD were performed by using a very short light pulse from a blue LED. The full duration of the pulse was 7 ns at 10% of the peak amplitude. The value was measured using a very fast timing phototube. The fall time and rise time of the HPD signal were 10 ns and 20 ns for HV=8 kV and at full depletion bias voltage. It will be shown later that there is a strong dependence of timing on bias for the "T-type" silicon because of the different charge carrier mobilities (the scale for electrons or holes transit time are 15 ps/um and 45 ps/um).

The repetition rate of the HPD signals was explored up to rates more than 30 MHz. It's important to note that this high rate capability is available without using special precautions such as are required in the case of regular photomultipliers. The current is delivered directly from the bias voltage power supply. Note that the transit time is <7 ns, so there is no pulse to pulse charge stored in the device at LHC rates. We also note that the HPD does not show any saturation for average output current values up to 10 mA.

The saturation effect manifests itself as the appearance of a tail in the signal shape for larger currents. This tail is dependent on the current density of the silicon and also on the value of the bias voltage. The effects will be discussed in more detail later.

Several measurements were performed to estimate the aging effect of the HPD. The photocathode was illuminated simultaneously by laser light (pulse mode) and by an LED (D.C. current).
(fig.5). To measure the output current of the HPD the zero potential side of the silicon was grounded through a 610 C Solid State Electrometer.
The LED intensity was adjusted to produce about 7 uA (25 mC/h) D.C. current from the HPD. The diameter of PC's illuminated area was 3 mm located at the geometrical center. The laser output HPD signal for the same area of illumination was then measured. A PIN photodiode signal was used to normalize the laser light pulse which had a spread of +/-3%. The ratio of the HPD signal over the PIN diode signal was measured with better than 1% accuracy. The result of the measurement is shown in fig.6. The gain drops after a steady charge of more than 50 mC is taken off the diode.

Another measurement of the aging was performed by using the setup shown in fig.7. The LED light (10 MHz, fig.8) was measured by HPD and PMT. The PMT worked with a very low gain and used as a reference for HPD pulse. A drop of the HPD amplitude was observed as a function of collected charge (fig.9). Both measurements are consistent if we take into account the illumination area which was of 7 mm diameter in the latter case.

Some estimation of the magnetic field influence on the HPD was done. The HPD was installed in 630 g transverse magnetic field. The gain of the HPD was measured without and with magnetic field (fig.10). We will show later that this curve is very sensitive to the magnetic field and can be used as a tool to check such effects. Many more magnetic field data were obtained for multipixel HPD but this will be the subject of a separate discussion.

We used an amplifier (also as preamplifier in part of the measurements) when working with a low light level signal. The ADC scale was calibrated to the number of photoelectrons with the goal to measure the lowest level of light which is possible to see with the HPD. The number of the photoelectrons can be extracted from the equation:

$$Npe \times aml.\ gain \times HPD\ gain = Q\ of\ ADC, \quad (1)$$

note that we know the gain of the HPD, amplifier and ADC scale in electrons. The number of photoelectrons can also be obtained by measuring the rms of the amplitude spectrum of the HPD illuminated by LED. A test is to compare this number with the number obtained from the mean value of the spectrum. The ratio of the two values should be 1 for the full HPD range. Any deviations present some apparatus effects.

The attempt to see a single photoelectron was successful (fig.11). We have used an ORTEC preamplifier in series with an amplifier with moderate bandwidth, high gain and low noise.

25 PIXELS HPD DEP

The front face of the HPD is shown in fig.12. The pixel size is 3.3 mm x 3.3 mm. The pixels are arranged in matrix 5 x 5 with a dead space between them of 0.2 mm. The distance between pixels and PC is 2.5 mm. The schematic view of the HPD is given in fig.13. The silicon in the HPD is oriented so that the layer facing the PC is T-type. The electrical signal of positive polarity was collected from the p-side which was grounded for high rate D.C. coupled operation.

The gain and uniformity of the pixels were tested (figs.14, 15) with results which are in very good agreement with the specifications. The output signal does not show any saturation for signals up to 100 mV/50 Ohm in amplitude.

The timing properties of the HPD were also studied. The output pulse shape is strongly dependent on the bias voltage. The rise time and full time (at the level 0.1 and 0.9 of the output signal peak amplitude) dependencies are shown in fig.16.

The rate dependence of the device was studied from 30 Hz to 30 MHz as shown in fig.17. Little rate dependence is observed indicating that the device can work in the LHC environment.

In fig.18 is shown the amplitude spectrum for different light levels up to 1000 photoelectrons. A non-gaussian high side tail evident in all spectra. In fig.19 the spectra at fixed light intensity as a function of HV are displayed. Clearly as HV increases the high side tail becomes more pronounced. In fig.20 we show the crosstalk starting from light on the fifth pixel in a row and moving to the first pixel in the row and plotting the spectrum obtained from the fifth pixel in all cases. The signal crosstalk falls off very rapidly as the illumination moves away indicating that the tail is due to localized sources.

Note also that the high side tail was much reduced in a second 25 pixel device which was tested. In addition, the fractional area taken by tail was largest at small values of incident light intensity. This behavior is what is expected if there are a bad vacuum in the device.

7 PIXEL HPD DEP

The gain, linearity, uniformity, timing and counting rate parameters look very similar to the 25 pixel HPD and are in very good agreement with specifications.

The amplitude spectra for this HPD are very different from 25 pixels HPD (fig.21). No high side tail is observed in the amplitude spectra under different HV (fig.26). However, this spectrum is still asymmetric, indicating that the effect is not wholly absent. The results of the measurements will be discussed below.

DISCUSSION

We have attempted to understand the HPD operation by collecting a full set of experimental data and by making model calculations [4].

We will discuss below the issues of direct relevance to the future HPD application for the CMS HCAL.

Our concerns now are about the following:
1.Timing.

We plan to work with an HPD of the T-type. The advantages are the following. The output signal is at ground so the readout is easy both for DC and pulse mode measurements. We have to use both these mode to accommodate wire source calibration. The T-type of HPD is also stated by the manufacturer to be more stable. The long term gain losses can also be corrected by increasing the high voltage.

The timing properties of the HPD are determinated by the type of charge carrier which are holes. The holes are less mobile than the electrons by a factor of approximately 3. The output signal duration is around 30 ns for 140 Volt bias. For the CMS application it should be less than the bunch crossing time of 25 ns. It's known that 10 keV photoelectrons penetrate into the silicon by only 1 um [3]. Therefore the thickness of the silicon can be significantly reduced without loss of HPD performance. Limitations which exist now on the allowed thickness are only technical. To improve the HPD timing it's possible to use 200 um silicon instead of 300 um in HPD. We believe it's possible to satisfy the CMS timing requirements by slightly changing the existing technology.

2. Another issue is the high side tail in the amplitude spectra.

Recall the shape of the single photoelectron distribution (fig.11). The tail of the distribution corresponds to several tens of a photoelectrons. This looks like a "shower" produced by the original single photoelectron. Let's consider possible reasons for this. The data do not favor mechanisms like optical feedback produced by low energy gammas from electrons scattering on the surface of the silicon. Such gammas should produce a very different angular distribution than that indicated in fig.20. The effect is also difficult to explain by the backscattering of the secondary electrons from the Si surface.

A reasonable explanation would be poor vacuum of the HPD as illustrated in fig.23. The photoelectrons. can ionize the residual gas in a collision between PC and silicon. The ionization potential is of order ten eV so the initial photoelectrons do not lose significant energy. The produced positive ion will accelerate in the electric field and can knock out several additional photoelectrons depending on the energy of the ion (around 10 for 10 keV ion energy, [5]). A time jitter of around 10 ns corresponds to the signals which produce the high side tail in the amplitude spectrum. In contrast, the gaussian part has a time jitter of about 1 ns. The calculations show that the 10 keV electron's transit time for 3 mm distance d (fig.23) is around 100 ps. A transit time of the ion will be more than 4.5 ns. The transit time of an oxygen ion will be 18 ns. Hence the calculations and the experimental data are consistent with the ion feedback model.

There is no getter in the HPD. Nevertheless a getter will be introduced in the final HPD design to avoid the possibility of outgassing just as in the case of regular phototubes.

The data obtained were simulated by Monte Carlo method. We fit the single photoelectron spectrum (fig.11) by a polynomial corresponding to the tail plus an exponential distribution mostly responsible for the main part of the single photoelectron distribution (SPD, fig.24). The obtained curves for different photoelectrons are in good agreement with the experimental data (fig.25). For the SPD the ratio of the area under the tail to the full area of the spectrum is 0.3%. The cut between the tail and the rest of the spectrum is shown as the arrow in fig.24. The analogical cuts were applied on the spectra with the observed tails for different amount of photoelectrons. The ratio of the tail to total area as a function of the mean number photoelectrons is shown in fig.27.

It's useful to note that the SPD shape can be used as very sensitive tool to check the HPD vacuum and we intend to use that shape in sorting the delivered HPD.

3. We have observed a clear mip separation from pedestal by using HPD in a beam test of an HCAL prototype module [6]. We also can demonstrate a single

photoelectron spectrum here. Our task now is to take such a data with "QIE" [7] readout both for DC and pulse mode.
A detailed description of the HPD study in a 5 Tesla magnetic field will be the subject of separate note. Our data show that the HPD can operate in the CMS magnet.

CONCLUSION

The HPD's are chosen as photodetectors for the HCAL subsystem of CMS. Some improvement must be done for the final transducer.

ACKNOWLEDGMENT

We appreciate useful discussions with V.Kubarovsky, and also the Monte Carlo results obtained by A.Volkov.

BIBLIOGRAPHY

1. The Hybrid Photomultiplier tubes (HPMT's), Catalog of DEP DELFT INSTRUMENTS Co.
2.Compact Muon Solenoid (CMS), Technical Proposal CERN/LHCC 94-38 LHCC/P1 15 December 1994.
3.S.Basa et al., Nucl. Instr. and Meth. A330, 1993, 93 - 99.
4. D. Green, Fermilab notes.
5. Physical constants. A.P.Babichev, N.A.Babushkina, A.M.Bratkovskiy at al. Under edition of I.S.Grigoriev, E.Z.Meilikhov. Moscow, Energoatomizdat, 1991, page 591.
6. P.Cushman et al. Comparison of Hybrid Photodiodes and Avalanche Photodiodes as candidate transducer for CMS HCAL. Preprint submitted to Elsevier Preprint, 3 September 1996.
7. G.W.Foster et al. A pipelined multiranging integrator and encoder ASIC for fast digitization of photomultiplier signals. Proc. 2nd Annual Conference on Electronics for Future Colliders. Chestnut Ridge, NY May 19-21 1992.

Figures.

1.The hybrid photodiode schematic view.
2.Setup to measure gain, linearity and nonuniformity of the HPD. HPD - hybrid photodiode, WLS - wave length shifter, PIN - photodiode, AW - attenuation wheel, LED - light emitted diode, ADC - analog digital converter.
3.Schematic view of the single channel HPD.
4.The dependence of the HPD's amplitude on: a) photocathode high voltage, b) silicon bias.
5.Setup for aging test. LED is working in DC mode.
6.The HPD relative gain vs integrated output charge.
7.Setup to measure aging in pulse mode. HP gen. - HEWLETT PACKARD generator, PMT - photomultiplier.
8.The oscilloscope traces of the HPD and HP generator's signals.
9.Loss of the HPD signal due to the integrated output charge.
10.The HPD amplitude vs high voltage with and without magnetic field.
11.Single photoelectron spectrum.
12.Front view of the 25 pixel HPD DEP. Pixel's size is 3.3x3.3 mm2.
13.The schematic view of the 25 pixel HPD DEP.
14.The amplitude of the pixel of the 25 pixel HPD DEP vs high voltage.
15.The spread of amplitude of the pixels. The fiber is exactly in the geometrical centre of the each pixel.
16.The rise time and the full time of the output HPD signals dependencies on bias voltage. High voltage fixed as -8 kV.
17.The oscilloscope traces of the HPD signals under 30 Hz and 30 MHz of frequency.
18 a,b. The amplitude spectra of the 25 pixel HPD under different light illumination.
19.The amplitude spectra of the central pixel of 25 pixel HPD vs high voltage. The number of the photoelectrons is around 60.
20.The amplitude spectra of the pixel #5d for fiber positioned on pixels ##5d,4d,3d,2d,1d. Each picture shows two measurements: one with light illumination and another, one without illumination.
21.The amplitude spectra of the 7 pixel HPD under different light illumination (for central pixel).
22.The amplitude spectra of the central pixel of 7 pixel HPD vs high voltage. The number of the photoelectrons is around 60.
23.Picture illustrating ion feedback in the HPD.
24.Approximated single photoelectron distribution (fig.11). The cut is shown by the location of the arrow.
25.The amplitude spectra of the 25 pixel HPD (DEP) obtained by Monte Carlo simulation.

26.The dependence of area under the tail over the full area in the spectrum on the number of photoelectrons. The number of photoelectrons is defined by the location of the maximum of the amplitude spectra.

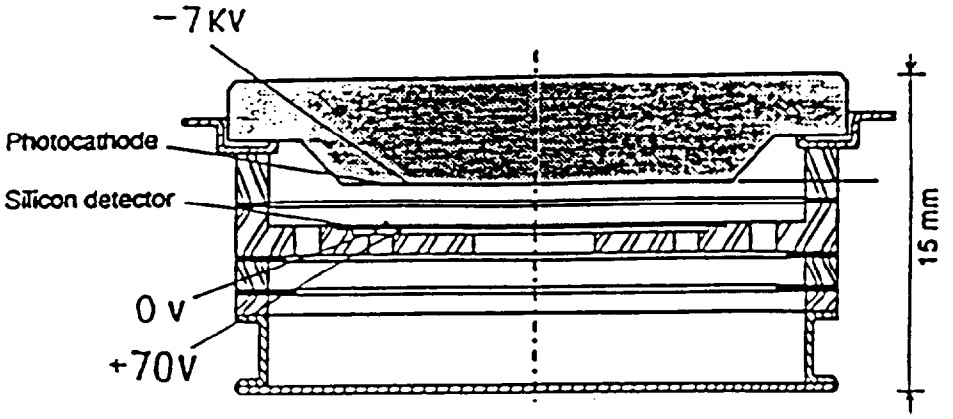

Fig.1.

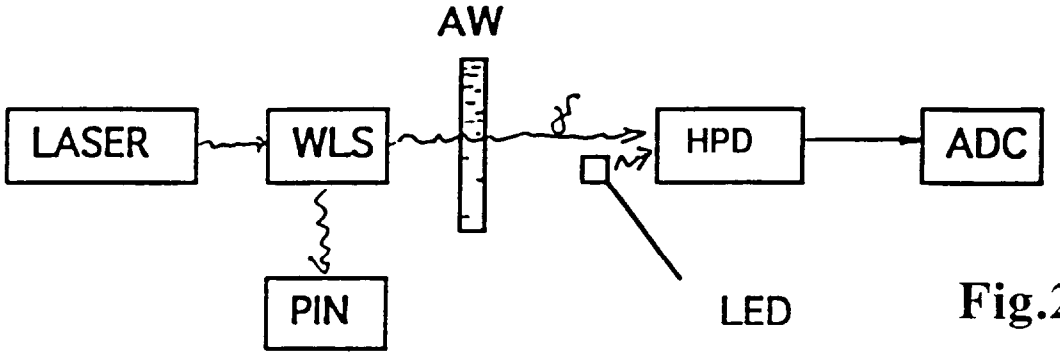

Fig.2.

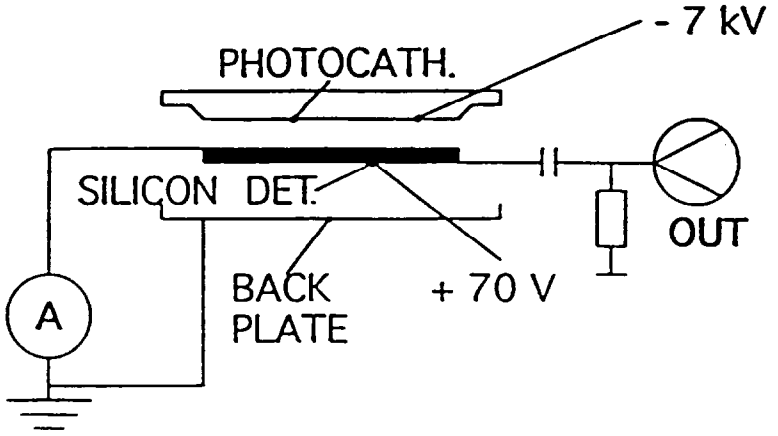

Fig.3.

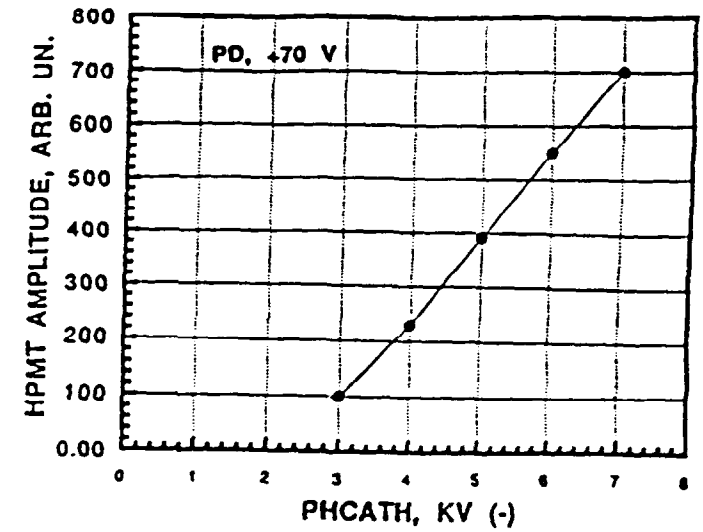
PD, +70 V
HPMT AMPLITUDE, ARB. UN.
800
700
600
500
400
300
200
100
0.00
0
1
2
3
4
5
6
7
8
PHCATH, KV (-)

a

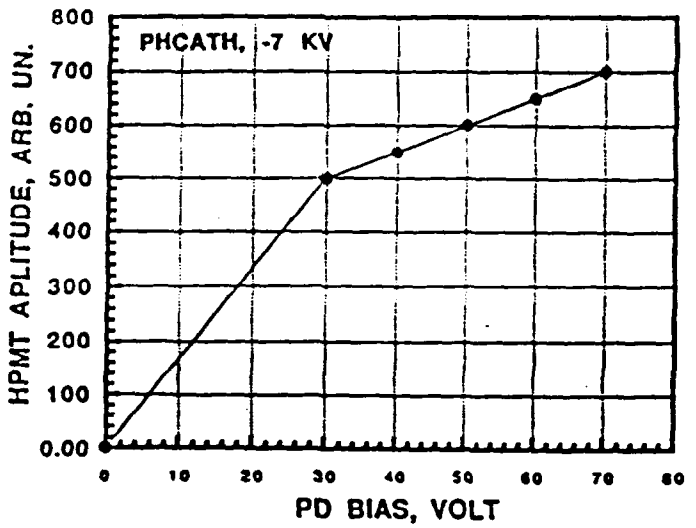
PHCATH, -7 KV
HPMT APLITUDE, ARB. UN.
800
700
600
500
400
300
200
100
0.00
0
10
20
30
40
50
60
70
80
PD BIAS, VOLT

b

Fig.4.

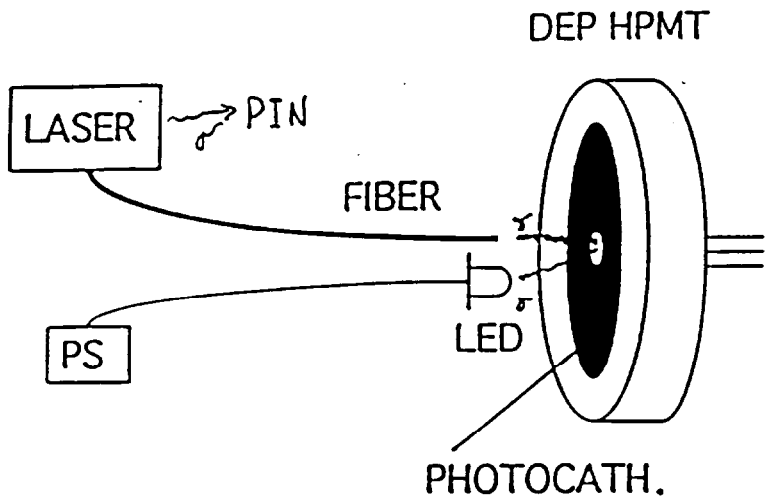
DEP HPMT
LASER
PIN
FIBER
LED
PS
PHOTOCATH.

Fig.5.

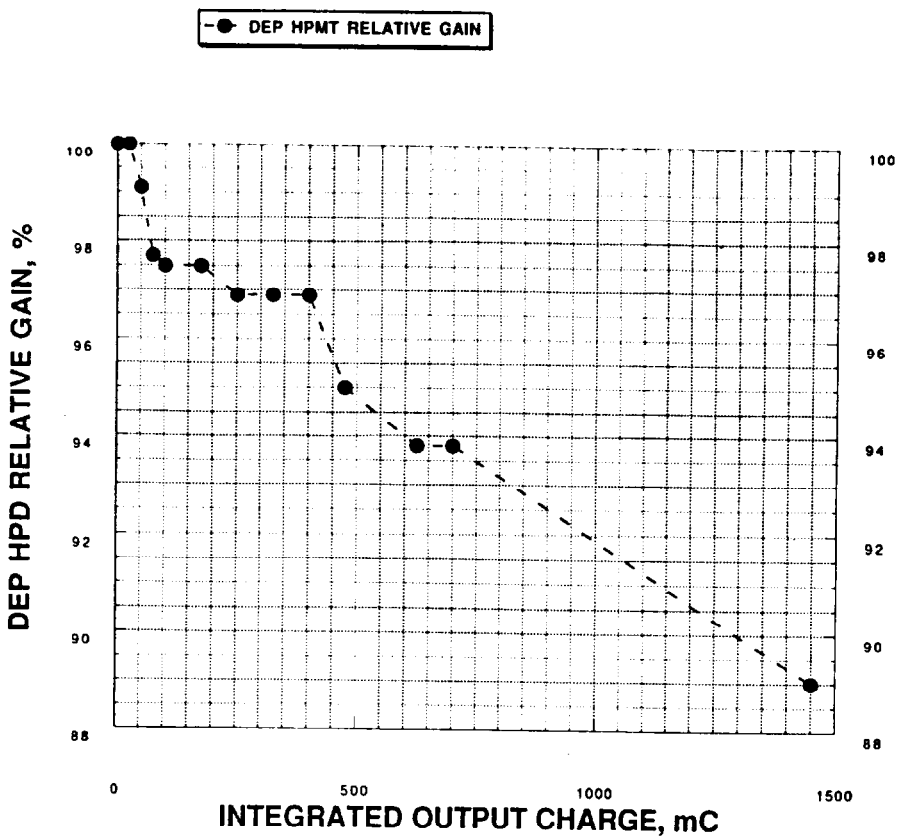
DEP HPMT RELATIVE GAIN
DEP HPD RELATIVE GAIN, %
100
98
96
94
92
90
88
0
500
1000
1500
INTEGRATED OUTPUT CHARGE, mC

Fig.6.

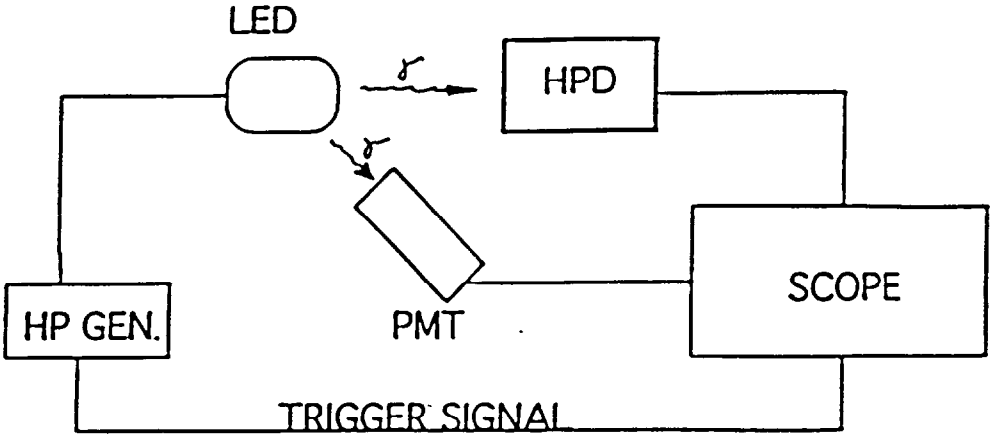

Fig.7.

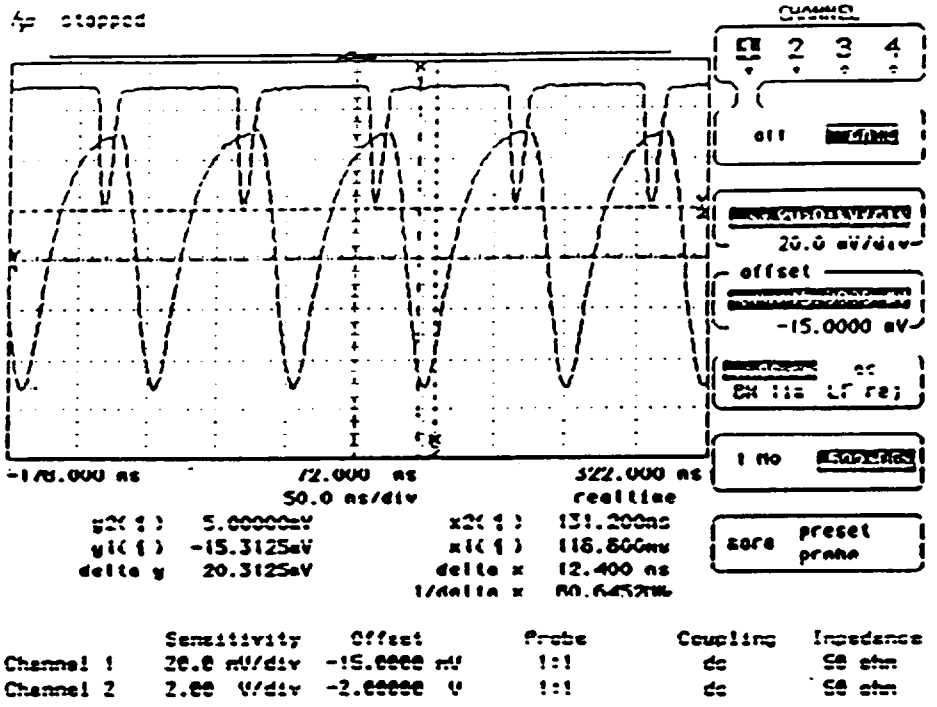

Fig.8.

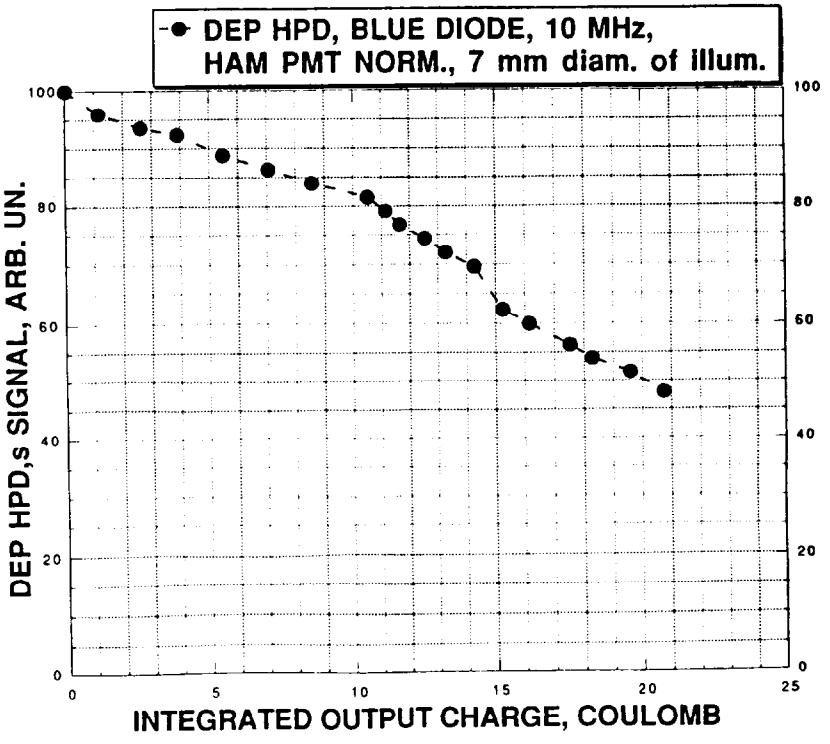

Fig.9.

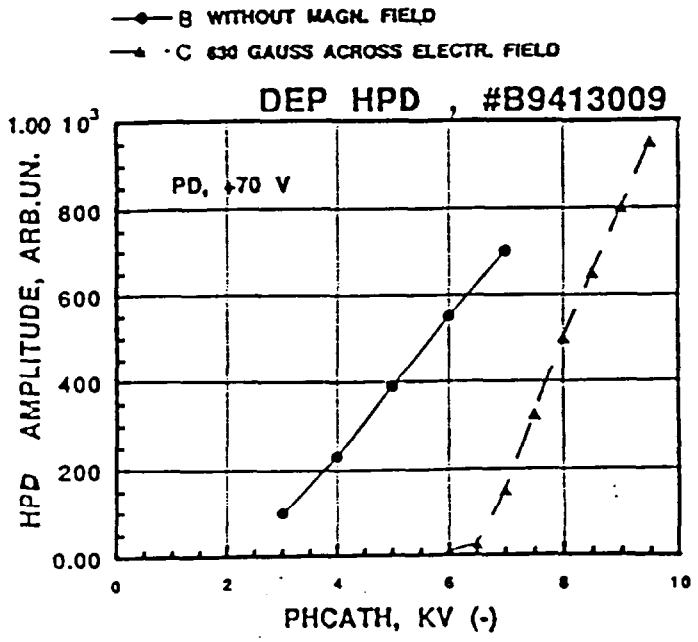

a)

Fig.10.

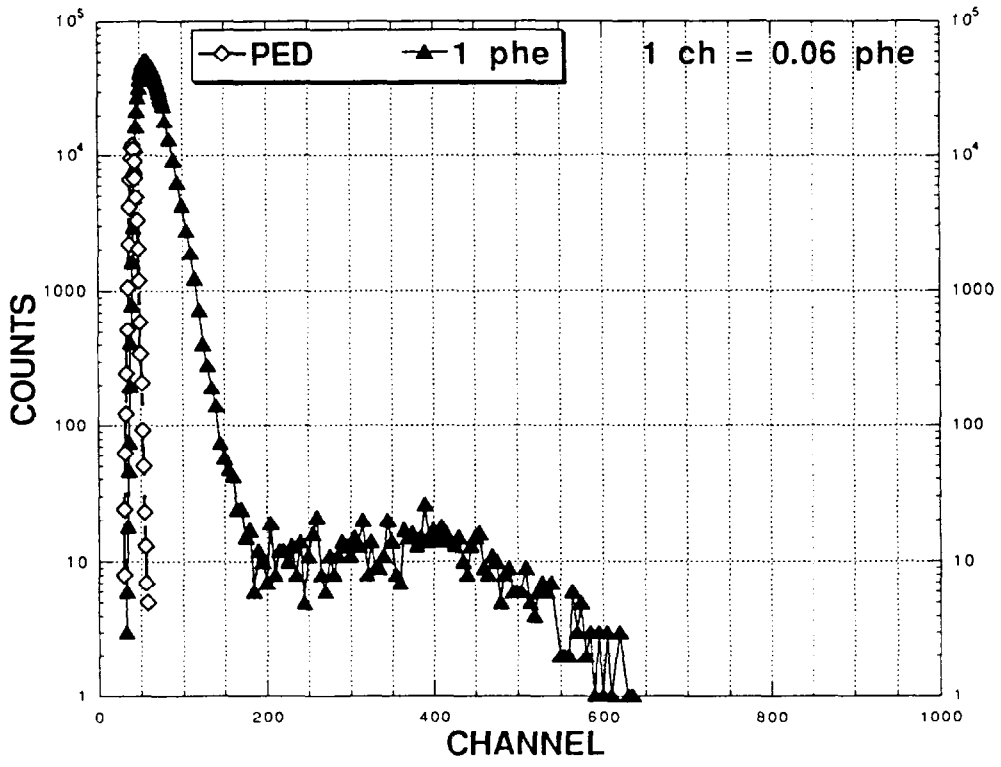

Fig.11.

25 PIXELS HPD DEP

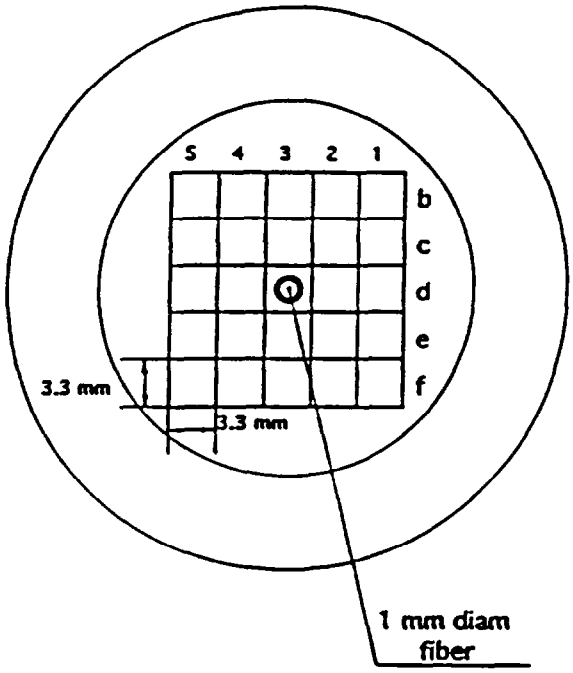

Fig.12.

25 pixels HPD DEP

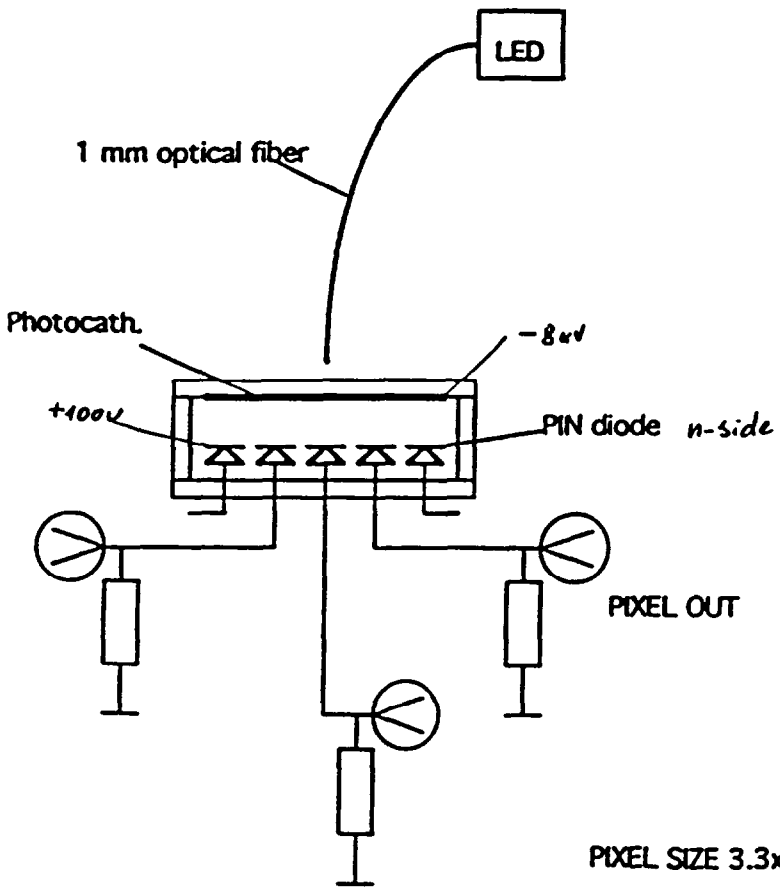

Fig.13.

PIXEL SIZE 3.3x3.3 mm2

GAP between PCath. and PIN diode is 2.5 mm.

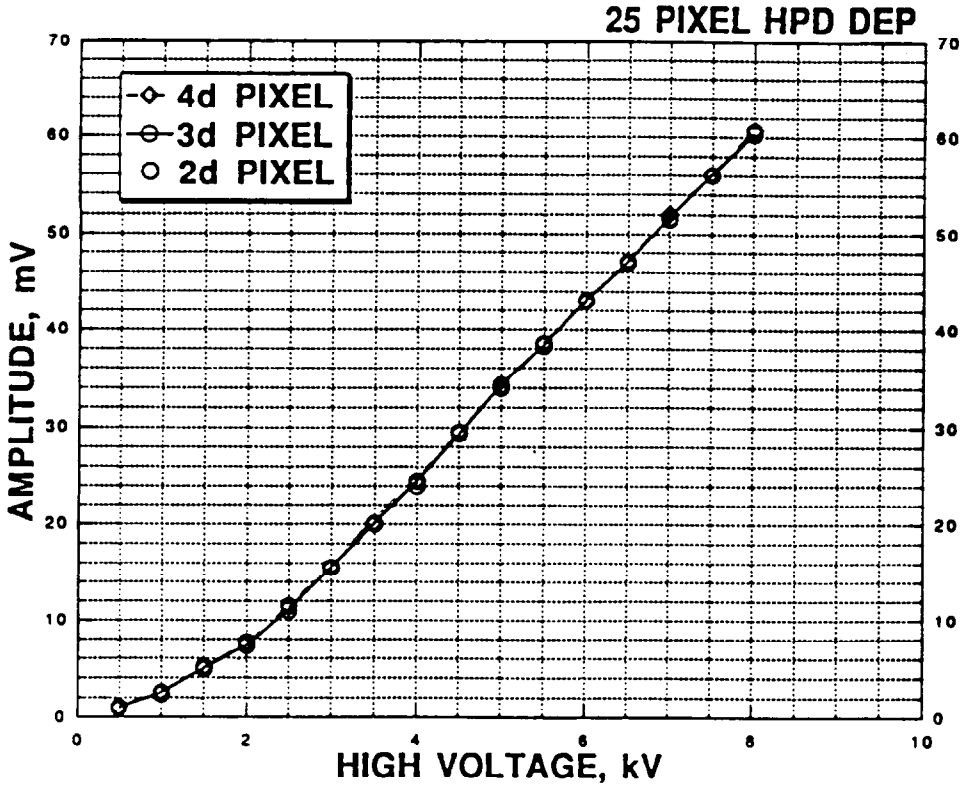
25 PIXEL HPD DEP
4d PIXEL
3d PIXEL
2d PIXEL
AMPLITUDE, mV
HIGH VOLTAGE, kV
0
10
20
30
40
50
60
70
0
2
4
6
8
10

Fig.14.

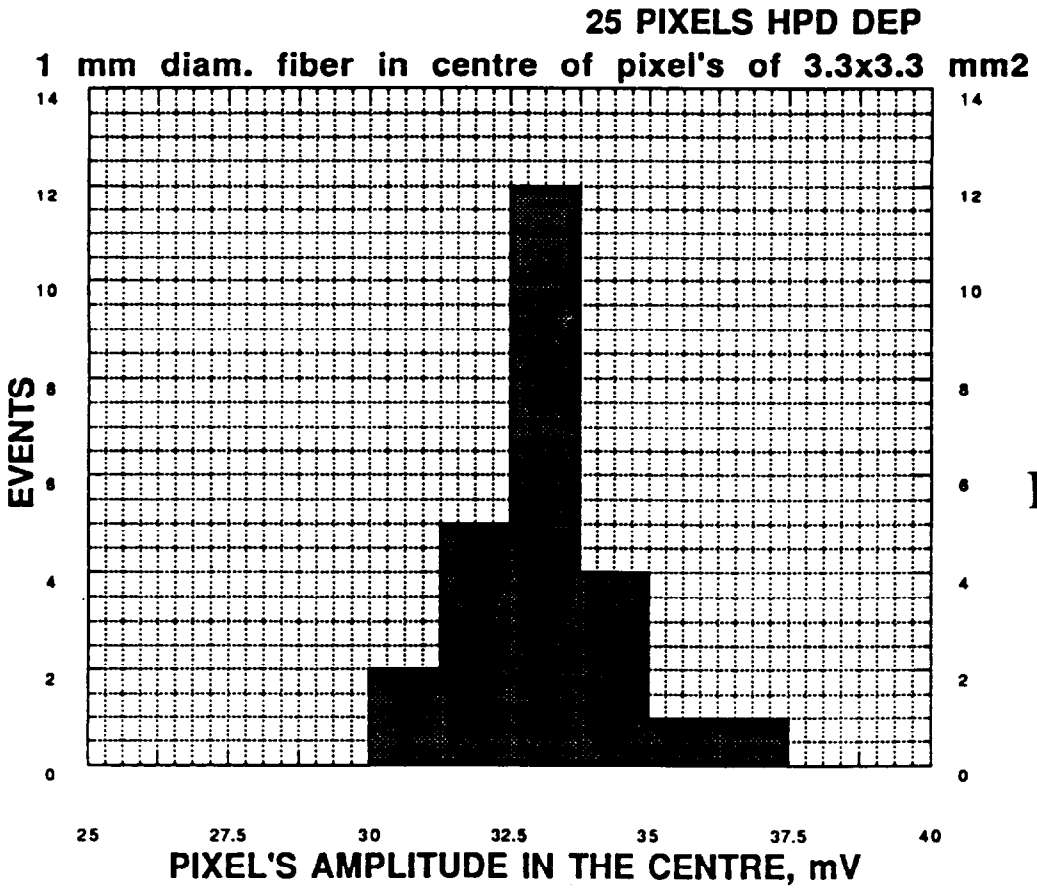
25 PIXELS HPD DEP
1 mm diam. fiber in centre of pixel's of 3.3x3.3 mm2
EVENTS
PIXEL'S AMPLITUDE IN THE CENTRE, mV
0
2
4
6
8
10
12
14
25
27.5
30
32.5
35
37.5
40

Fig.15.

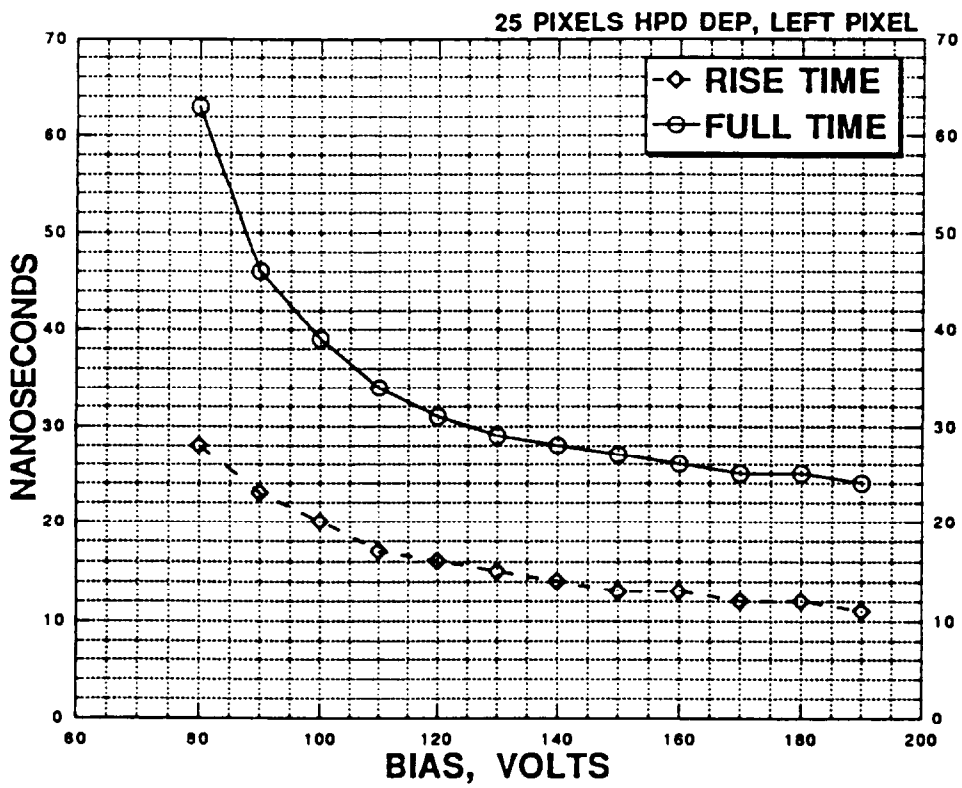
25 PIXELS HPD DEP, LEFT PIXEL
RISE TIME
FULL TIME
NANOSECONDS
BIAS, VOLTS
0
10
20
30
40
50
60
70
60
80
100
120
140
160
180
200

Fig.16.

30 Hz

Printed: 11 FEB 1997 at 19:50:15

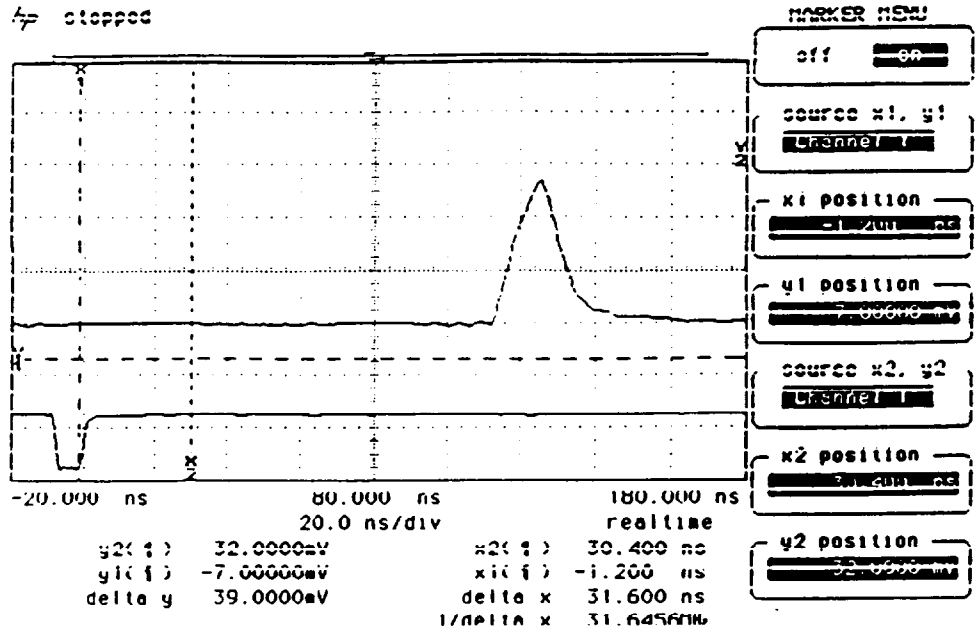

	Sensitivity	Offset	Probe	Coupling	Impedance
Channel 1	10.0 mV/div	10.0000 mV	1:1	dc	50 ohm
Channel 4	5.00 V/div	19.7500 V	10:1	dc	50 ohm

Trigger Mode: Edge

Printed: 11 FEB 1997 at 19:53:03

30 MHz

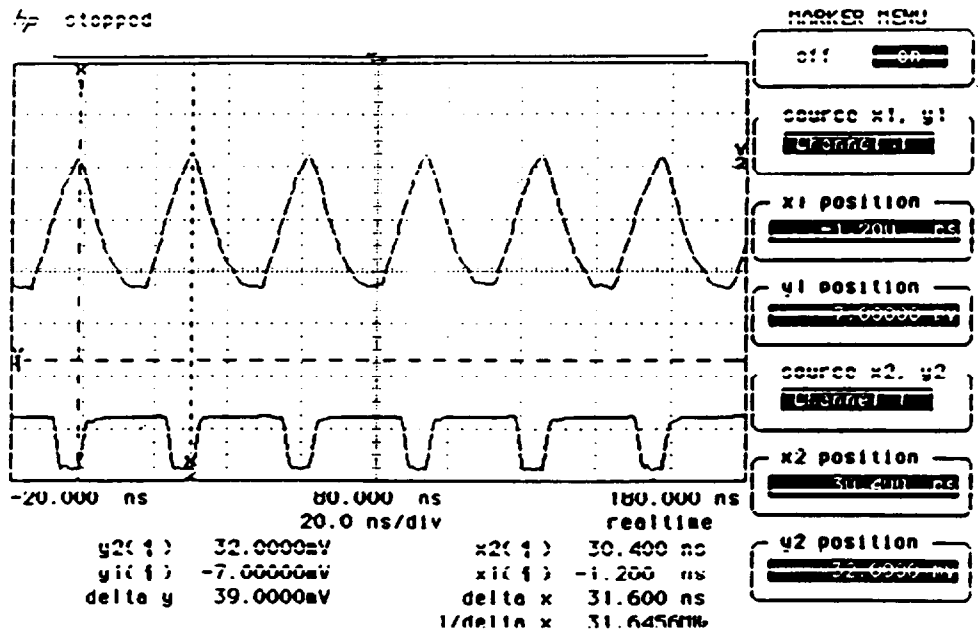

	Sensitivity	Offset	Probe	Coupling	Impedance
Channel 1	10.0 mV/div	10.0000 mV	1:1	dc	50 ohm
Channel 4	5.00 V/div	19.7500 V	10:1	dc	50 ohm

Trigger Mode: Edge
On the Positive Edge of Channel4
Trigger Level(s)
Channel4 = 2.50000 V (noise reject OFF)
HoldOff = 40.000 ns

Fig.17.

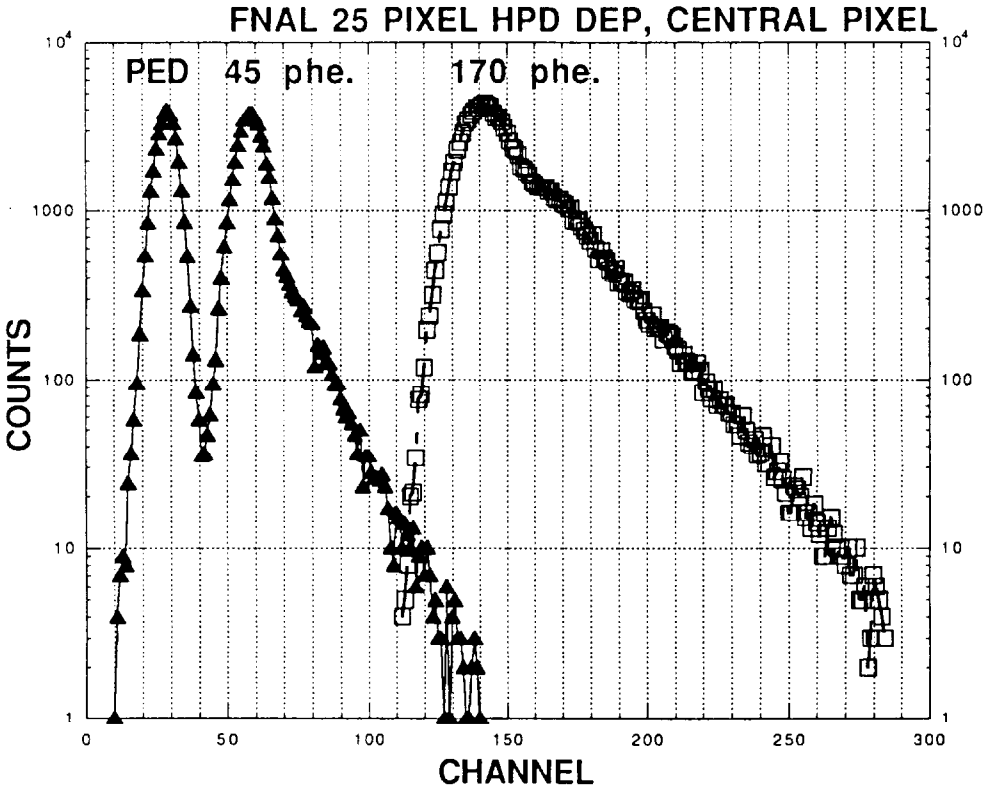
FNAL 25 PIXEL HPD DEP, CENTRAL PIXEL
PED
45 phe.
170 phe.
COUNTS
CHANNEL
10^4
1000
100
10
1
0
50
100
150
200
250
300

Fig.18.a

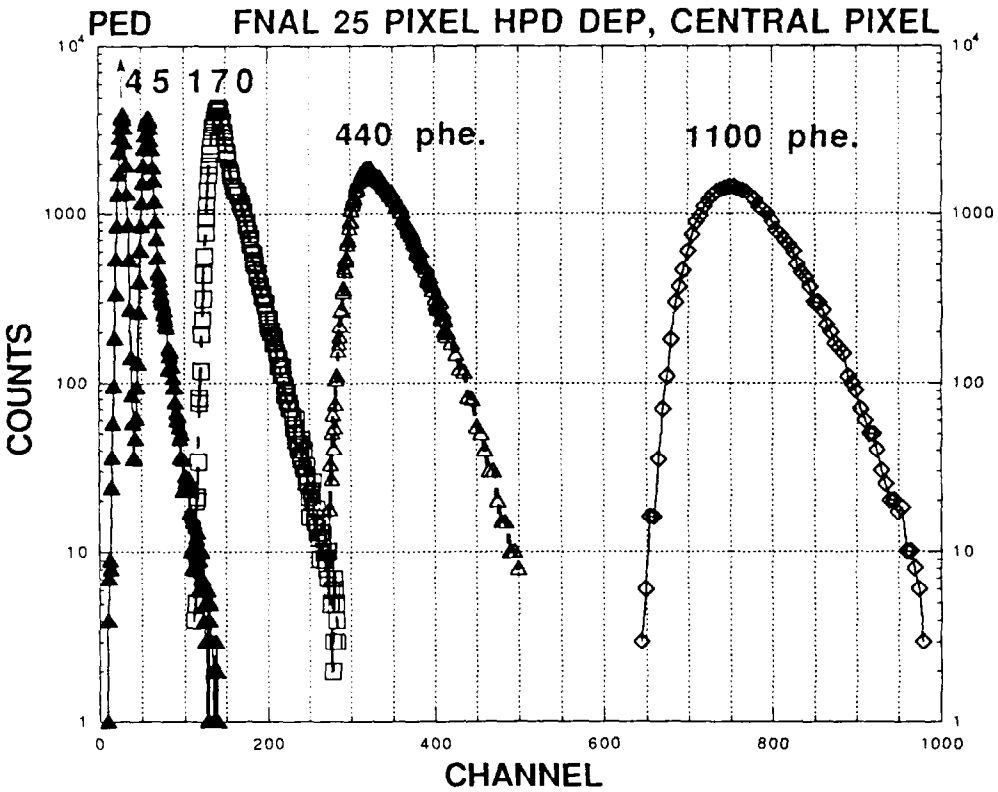
PED
FNAL 25 PIXEL HPD DEP, CENTRAL PIXEL
45 170
440 phe.
1100 phe.
COUNTS
CHANNEL
10^4
1000
100
10
1
0
200
400
600
800
1000

Fig.18. b.

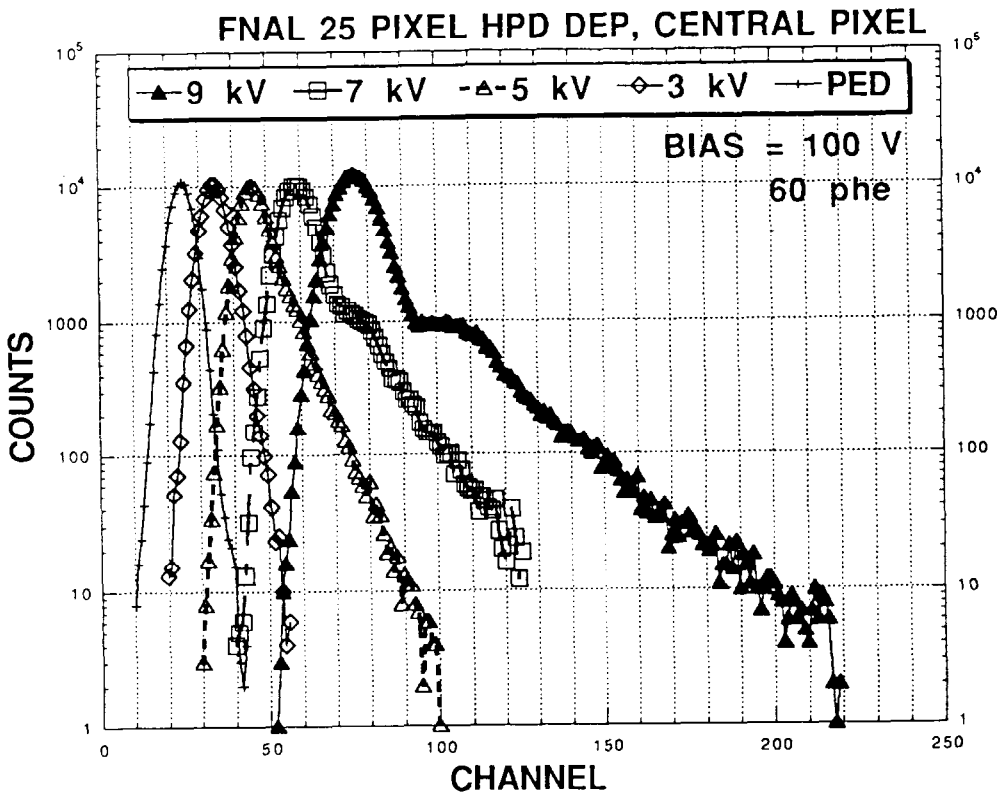
FNAL 25 PIXEL HPD DEP, CENTRAL PIXEL
9 kV
7 kV
5 kV
3 kV
PED
BIAS = 100 V
60 phe
COUNTS
CHANNEL
10^5
10^4
1000
100
10
1
0
50
100
150
200
250

Fig.19.

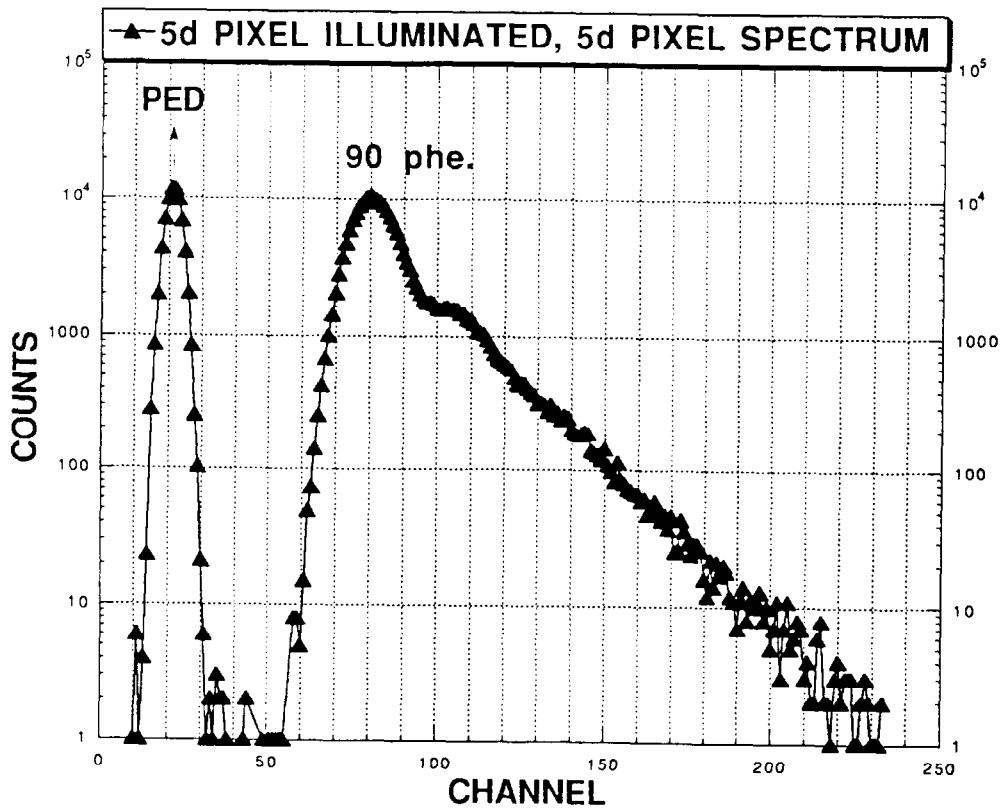
5d PIXEL ILLUMINATED, 5d PIXEL SPECTRUM
PED
90 phe.
COUNTS
CHANNEL
10^5
10^4
1000
100
10
1
0
50
100
150
200
250

Fig.20. *a*.

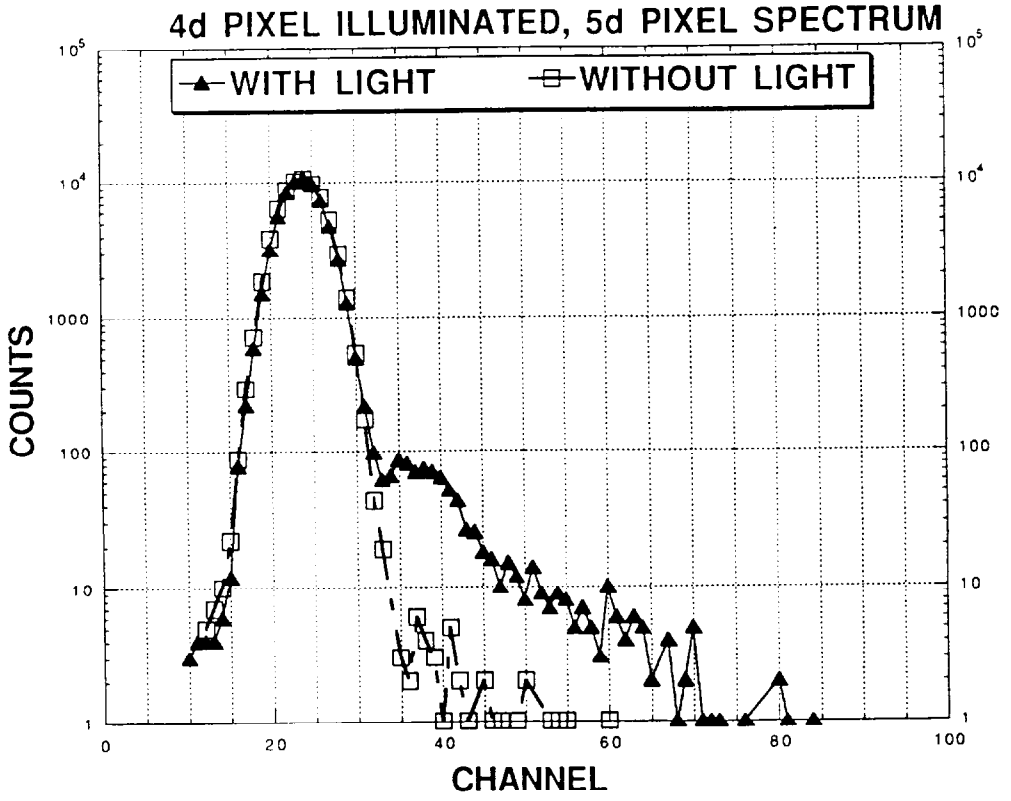
4d PIXEL ILLUMINATED, 5d PIXEL SPECTRUM
WITH LIGHT
WITHOUT LIGHT
COUNTS
CHANNEL
10^5
10^4
1000
100
10
1
0
20
40
60
80
100

Fig.20.b.

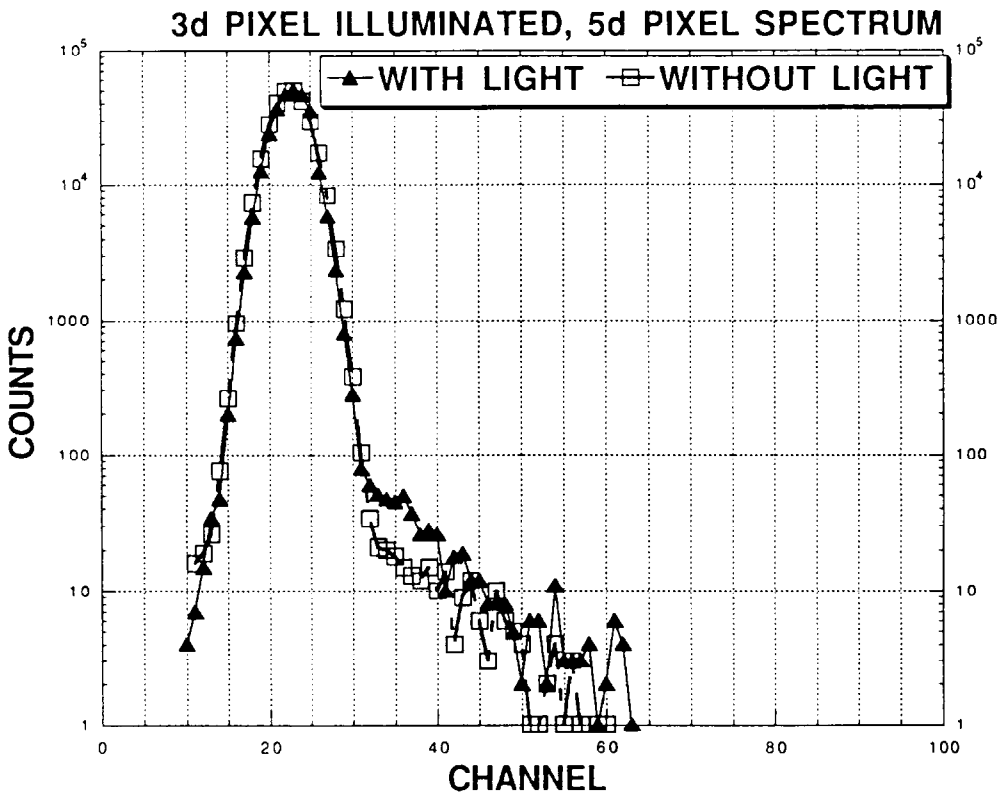
3d PIXEL ILLUMINATED, 5d PIXEL SPECTRUM
WITH LIGHT
WITHOUT LIGHT
COUNTS
CHANNEL
10^5
10^4
1000
100
10
1
0
20
40
60
80
100

Fig.20.c.

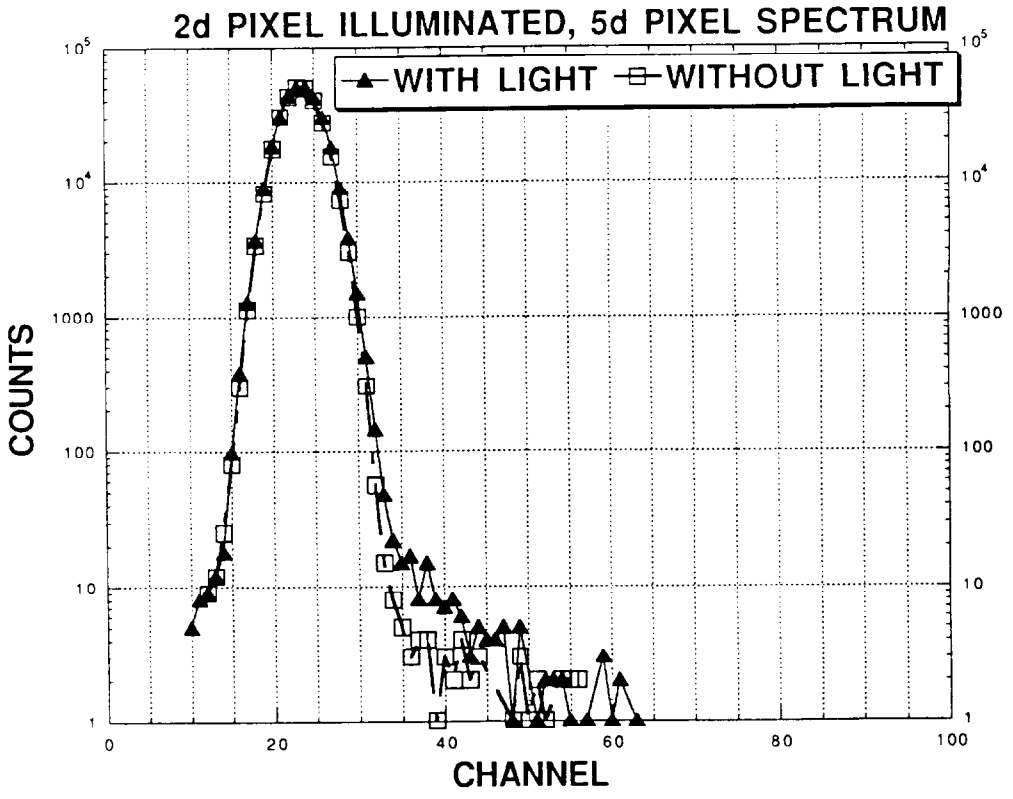
2d PIXEL ILLUMINATED, 5d PIXEL SPECTRUM
WITH LIGHT
WITHOUT LIGHT
COUNTS
CHANNEL
10^5
10^4
1000
100
10
1
0
20
40
60
80
100

Fig.20. *d*.

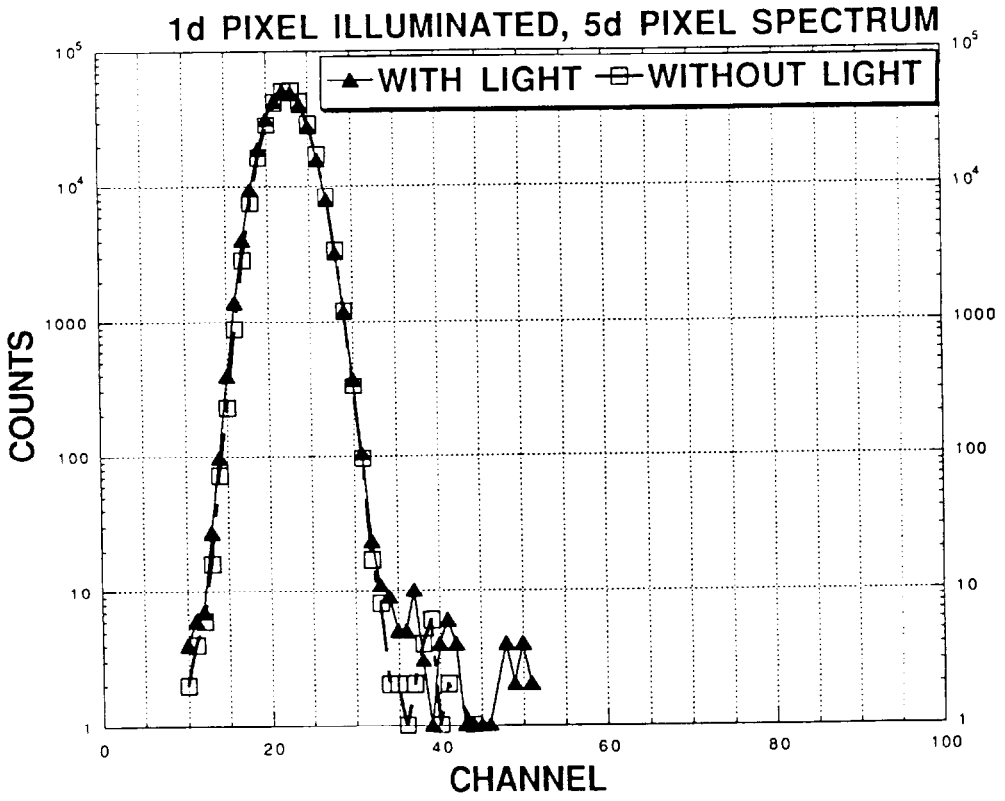
1d PIXEL ILLUMINATED, 5d PIXEL SPECTRUM
WITH LIGHT
WITHOUT LIGHT
COUNTS
CHANNEL
10^5
10^4
1000
100
10
1
0
20
40
60
80
100

Fig.20.e.

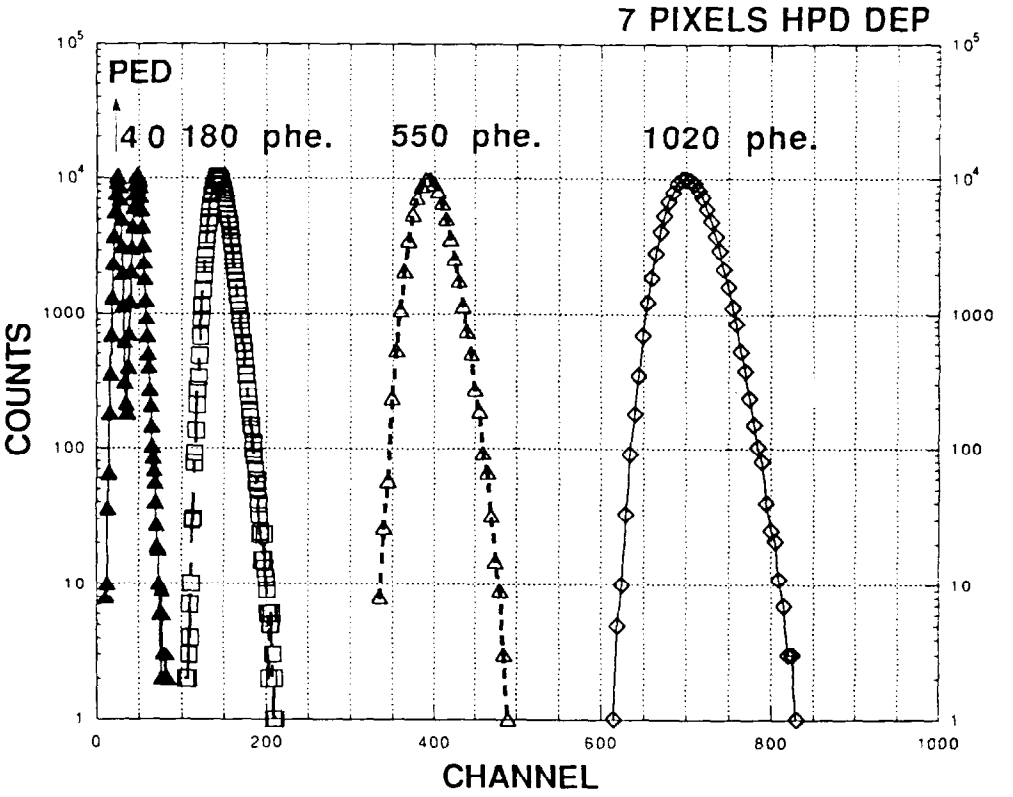
7 PIXELS HPD DEP
PED
4 0
180 phe.
550 phe.
1020 phe.
COUNTS
CHANNEL
10^5
10^4
1000
100
10
1
0
200
400
600
800
1000

Fig.21.

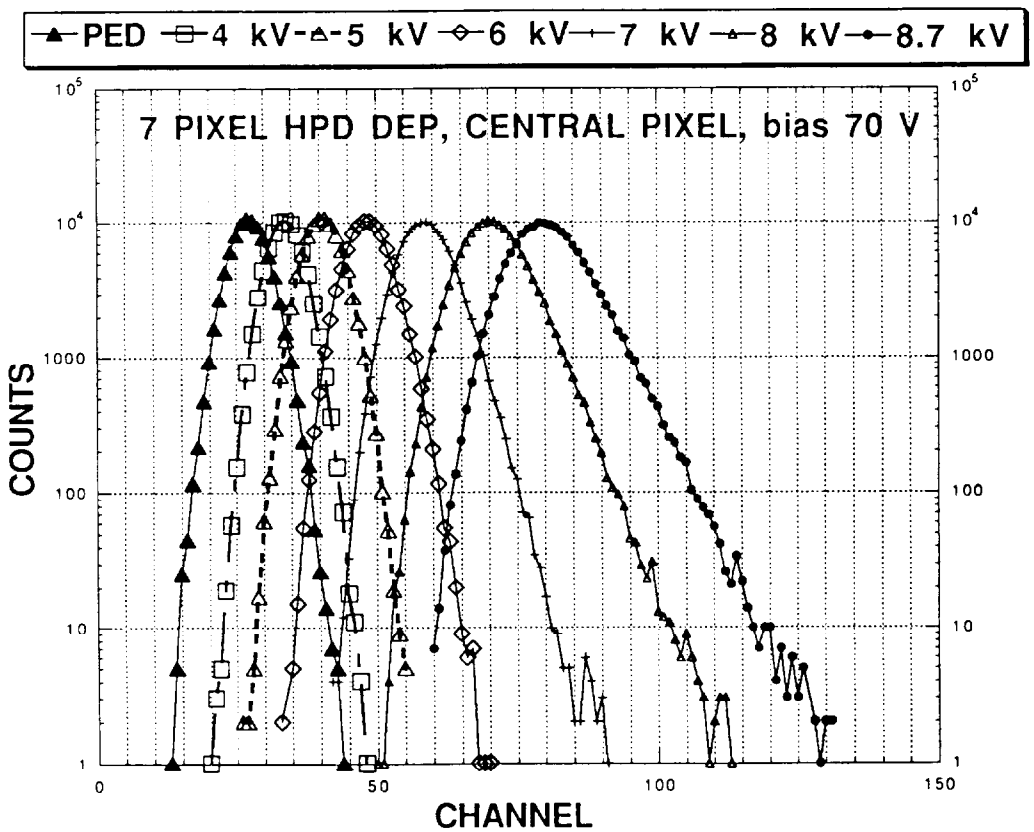
PED
4 kV
5 kV
6 kV
7 kV
8 kV
8.7 kV
7 PIXEL HPD DEP, CENTRAL PIXEL, bias 70 V
COUNTS
CHANNEL
10^5
10^4
1000
100
10
1
0
50
100
150

Fig.22.

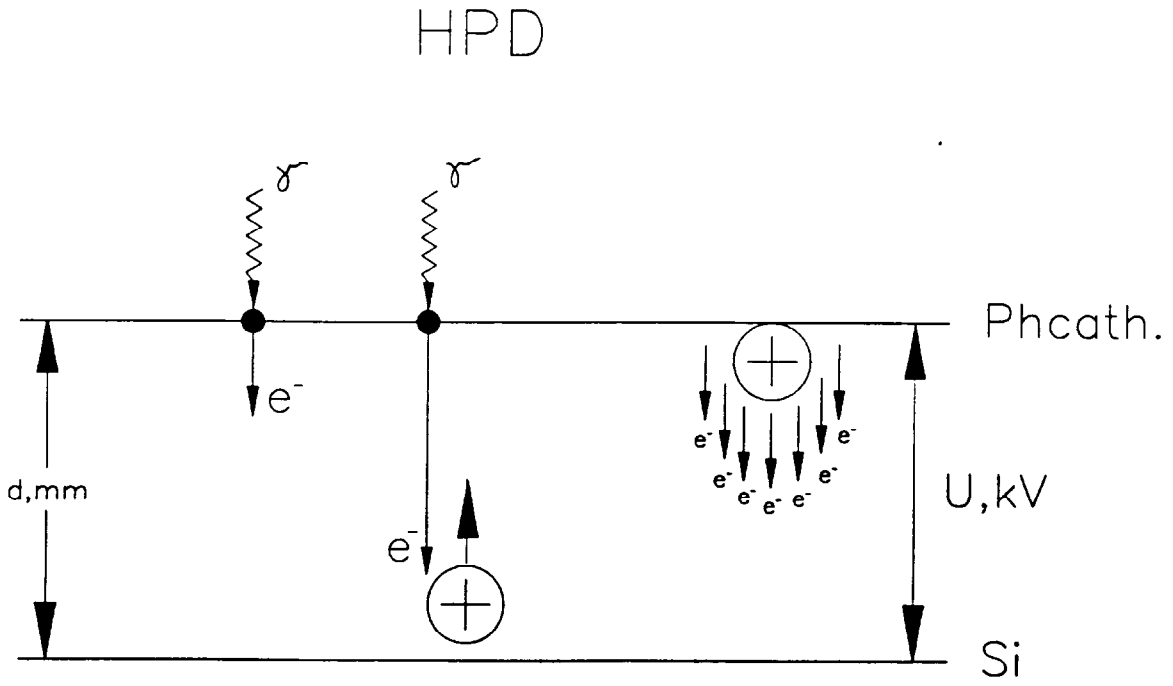

Fig.23.

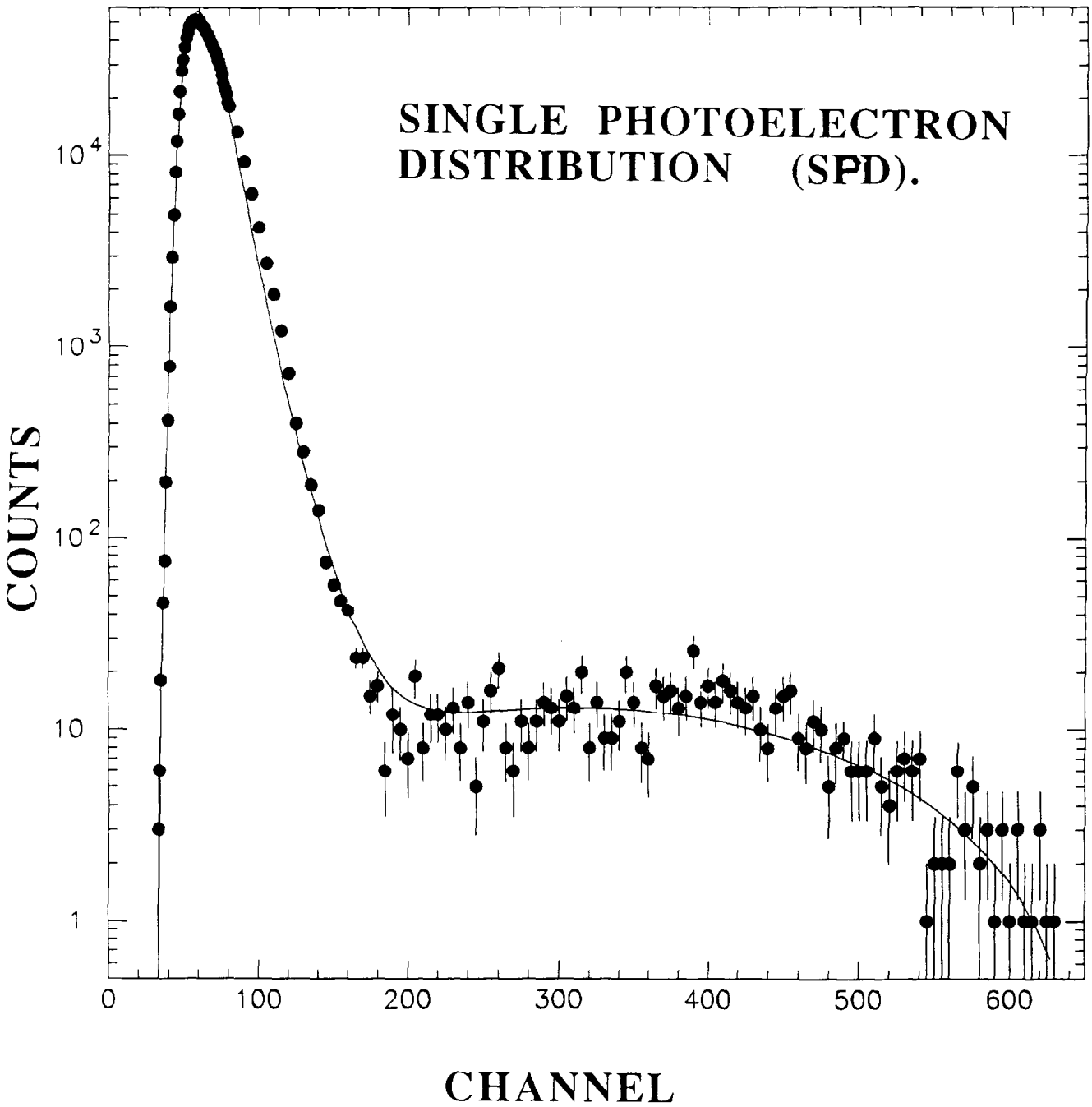
SINGLE PHOTOELECTRON
DISTRIBUTION (SPD).
COUNTS
CHANNEL
10^4
10^3
10^2
10
1
0
100
200
300
400
500
600

Fig.24.

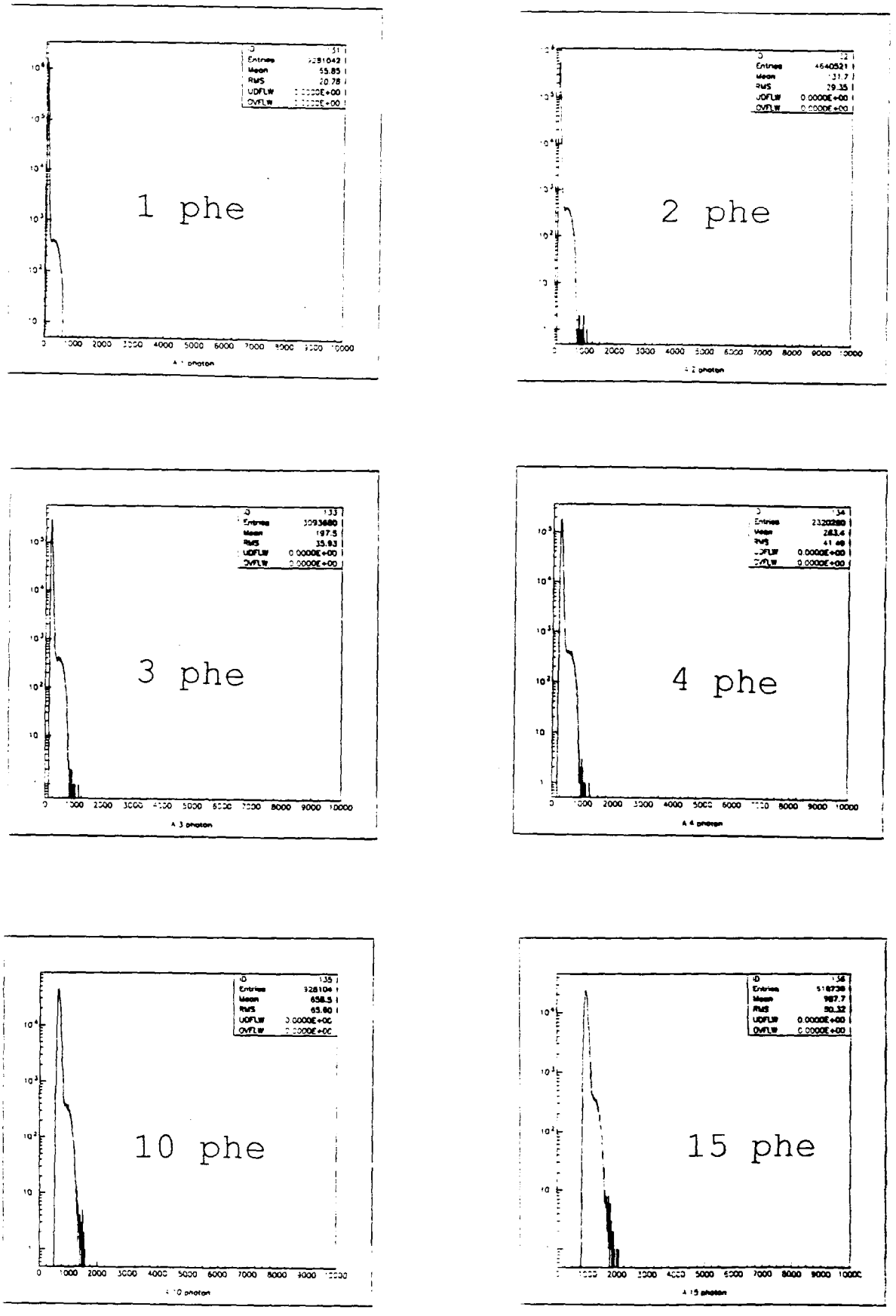

Fig.25.

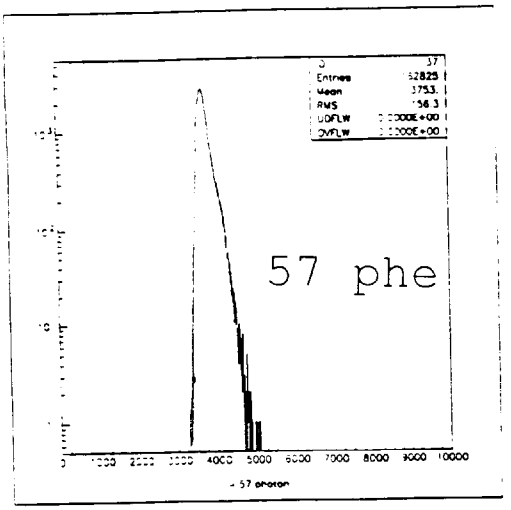
57 phe
Entries
Mean
RMS
UDFLW
OVFLW
1000 2000 3000 4000 5000 6000 7000 8000 9000 10000

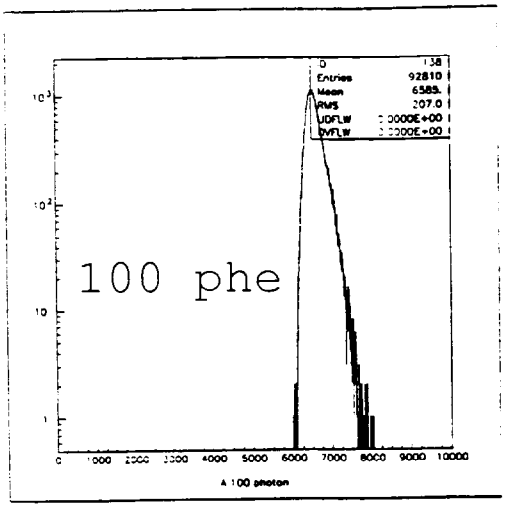
100 phe
Entries 92810
Mean 6585.
RMS 207.0
UDFLW
OVFLW
1000 2000 3000 4000 5000 6000 7000 8000 9000 10000
A 100 photon

Fig.25.

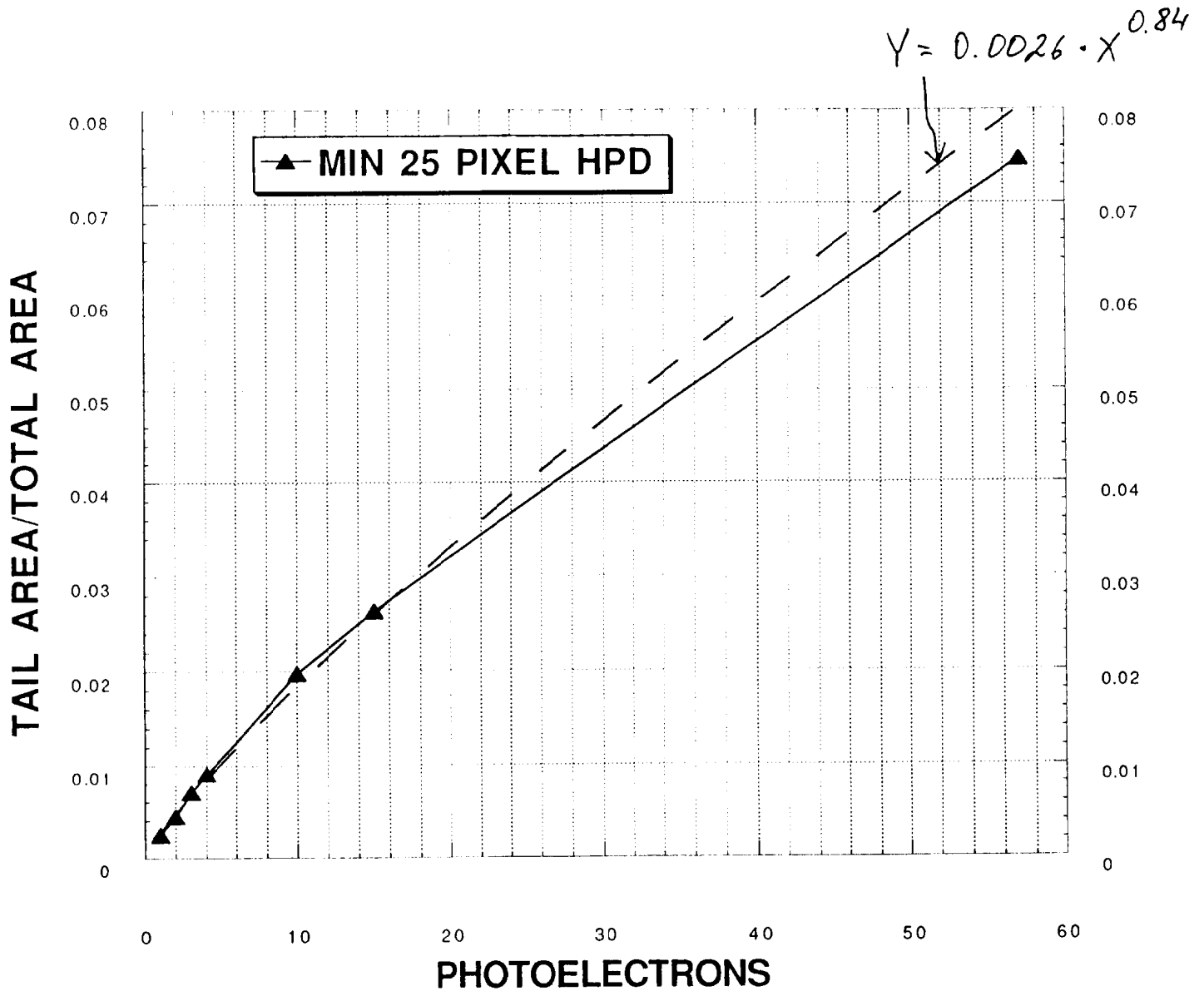
Y = 0.0026 · X^0.84
MIN 25 PIXEL HPD
TAIL AREA/TOTAL AREA
PHOTOELECTRONS
0
0.01
0.02
0.03
0.04
0.05
0.06
0.07
0.08
0
10
20
30
40
50
60

Fig.26.